Miner Deposita (2017) 52:1179–1190
DOI 10.1007/s00126-017-0715-y

ARTICLE

In situ SIMS U-Pb dating of hydrothermal rutile: reliable age for the Zhesang Carlin-type gold deposit in the golden triangle region, SW China

Qiaohui Pi[1,2] · Ruizhong Hu[1] · Bin Xiong[2] · Qiuli Li[3] · Richen Zhong[4]

Received: 24 April 2016 / Accepted: 12 December 2016 / Published online: 1 February 2017
© Springer-Verlag Berlin Heidelberg 2017

Abstract The contiguous region between Guangxi, Guizhou, and Yunnan, commonly referred to as the Golden Triangle region in SW China, hosts many Carlin-type gold deposits. Previously, the ages of the gold mineralization in this region have not been well constrained due to the lack of suitable minerals for radiometric dating. This paper reports the first SIMS U–Pb age of hydrothermal rutile crystals for the Zhesang Carlin-type gold deposit in the region. The hydrothermal U-bearing rutile associated with gold-bearing sulfides in the deposit yields an U-Pb age of 213.6 ± 5.4 Ma, which is within the range of the previously reported arsenopyrite Re–Os isochron ages (204 ± 19 to 235 ± 33 Ma) for three other Carlin-type gold deposits in the region. Our new and more precise rutile U-Pb age confirms that the gold mineralization was contemporaneous with the Triassic W–Sn mineralization and associated granitic magmatism in the surrounding regions. Based on the temporal correlation, we postulate that coeval granitic plutons may be present at greater depths in the Golden Triangle region and that the formation of the Carlin-type gold deposits is probably linked to the coeval granitic magmatism in the region. This study clearly demonstrates that in situ rutile U–Pb dating is a robust tool for the geochronogical study of hydrothermal deposits that contain hydrothermal rutile.

Keywords Rutile U-Pb dating · Carlin-type gold deposit · Granitic magmatism · Golden triangle in SW China · Indosinian (Triassic) orogeny

Editorial handling: H. Chen

✉ Ruizhong Hu
huruizhong@vip.gyig.ac.cn

[1] State Key Laboratory of Ore Deposit Geochemistry, Institute of Geochemistry, Chinese Academy of Sciences, Guiyang 550081, China

[2] Guangxi Key Laboratory of Exploration for Hidden Metallic Ore Deposits, Guilin University of Technology, Guilin 541004, China

[3] State Key Laboratory of Lithospheric Evolution, Institute of Geology and Geophysics, Chinese Academy of Sciences, Beijing 100029, China

[4] Civil and Environmental Engineering School, University of Science and Technology of Beijing, Beijing 100083, China

Introduction

The Carlin-type gold deposits, which are among the largest hydrothermal gold deposits in the world (Kesler et al. 2005), are present in Nevada, USA, and southwestern China (Su et al. 2008, 2009a, b, 2012; Tretbar et al. 2000; Hu et al. 2002; Arehart et al. 2003; Kesler et al. 2005; Cline et al. 2005; Muntean et al. 2011; Hu and Zhou 2012). This type of gold deposit is characterized by low-temperature alteration such as decarbonation, argillization, sulfidation, and silicification, by the association of Au with As, Sb, Hg, and Tl, and by the occurrences of invisible gold within arsenian pyrite crystals (Hofstra and Cline 2000; Hall et al. 2000; Hu et al. 2002). Gold precipitation is thought to have taken place during the sulfidation of iron-rich carbonates (Cline et al. 2005; Su et al. 2008).

Reliable ages for the Carlin-type gold deposits are critical for a better understanding of gold deposition and its relationship to regional geological processes such as metamorphism and magmatism. Various techniques have been used to determine the ages of the Carlin-type gold deposits in Nevada (Arehart et al. 2003). It was suggested that the Carlin-type gold deposits in Nevada formed between ~33 and ~40 Ma, based on Rb–Sr dating of galkhaite (Tretbar et al. 2000), Ar–Ar dating of adularia (Hall et al. 2000), and fission track dating

of apatite (Chakurian et al. 2003). It was also suggested that the ore formation took place during a tectonic transition from compression to extension, based on the presence of broadly coeval granitoids in the region (Arehart et al. 2003; Cline et al. 2005).

The ages of the Carlin-type gold deposits in the contiguous region between Guangxi, Guizhou, and Yunnan, the so-called Golden Triangle region in southwestern China, have not been well constrained due to the lack of suitable minerals for radiometric dating. A number of isotopic dating methods, such as Rb-Sr and Re-Os of sulfides, ^{40}Ar–^{39}Ar of sericite, and Rb-Sr of inclusion fluids, have been applied to the Carlin-type gold deposits in the Golden Triangle region, but the results are highly variable, ranging from ~80 to ~270 Ma (Hu et al. 1995, 2002; Su et al. 1998, 2009a; Chen et al. 2009, 2015). The extremely large variation is mainly from the Rb-Sr isochron ages of sulfides and fluid inclusions that are not reliable for dating hydrothermal deposits. For the sulfide Rb-Sr method, the problem is because both Rb and Sr are not hosted in the sulfide structure but mainly in silicate mineral inclusions of different origins. For the fluid-inclusion Rb-Sr method, the problem is due to the presence of multiple generations of fluid inclusions including secondary fluid inclusions in the samples. Excluding the data from these unreliable methods, the results from the other methods give a more restricted age range from ~195 to 235 Ma for the Carlin-type gold deposits in the Golden Triangle region in SW China (Chen et al. 2009, 2015). The sericite in the quartz veins of the Lannigou Carlin-type gold deposit in the region yielded a precise $^{40}Ar/^{39}Ar$ plateau age of 194.6 ± 2 Ma (Chen et al. 2009). The arsenopyrite crystals from the Lannigou, Jinya, and Shuiyindong Carlin-type gold deposits in the region yielded the less precise Re-Os isochron ages of 204 ± 19, 206 ± 22, and 235 ± 33 Ma, respectively (Chen et al. 2015).

Rutile (TiO_2) commonly occurs as a minor phase not only in magmatic and metamorphic rocks but also in hydrothermal alteration assemblages. It contains trace amounts of U in the structure (usually 0.1 to 10 s ppm^{-1}), enough for U-Pb isotope determination (Li et al. 2003, 2011; Meinhold 2010). Rutile has a closure temperature of >500°C for U-Pb diffusion (Vry and Baker 2006; Kooijman et al. 2010). These two properties together make rutile a useful geochronometer. As a result, rutile has been used to date magmatic and metamorphic rocks by many researchers (Bibikova et al. 2001; Hirdes and Davis 2002; Li et al. 2003, 2011) and to date hydrothermal deposits by a few researchers (Doyle et al. 2015).

We have employed in situ SIMS U–Pb dating of hydrothermal rutile to determine the age of the Zhesang Carlin-type gold deposit in the Golden Triangle region in SW China. This is the first time that this method is applied to the study of hydrothermal deposits in China. The new age and its significance in regional metallogeny are the main focusses of the paper.

Geological background

Regional geology

The South China Block consists of the Yangtze Craton to the north and the Cathaysian Block to the south (Fig. 1). The South China Block, the North China Craton, and the Indochina Block were amalgamated in the Mesozoic (Zhou et al. 2006; Wang et al. 2007). A lot of Carlin-type gold deposits are present in a contiguous region between Yunnan, Guizhou, and Guangxi Provinces in the southwestern part of the Yangtze Craton (Tu 1992; Hu et al. 2002). This region is commonly referred to as the Golden Triangle Region. These deposits have proven gold reserves of ca. ~800 t at an average grade of 4.5 g t^{-1} Au.

The basement of the Yangtze Craton is composed of Late Archean metamorphic rocks in the north and younger, only weakly metamorphosed Mesoproterozoic-Neoproterozoic meta-sedimentary rocks in the west and east, intruded by abundant Neoproterozoic igneous rocks in the west (Zhou et al. 2002). The sedimentary cover of the Yangtze Craton consists mainly of a thick Cambrian to Triassic carbonates and shales sequence of marine origin, and Jurassic, Cretaceous, and Cenozoic strata of continental facies (Yan et al. 2003). The Yanshanian (Jurassic to Cretaceous) and Indosinian (Triassic) magmatism produced voluminous granitic plutons and many associated W-Sn ore deposits within the Cathaysian Block and in the southernmost part of the Golden Triangle Region in the SW part of the Yangtze Craton (Hu and Zhou 2012; Hu et al. 2012a, b; Mao et al. 2013).

Deposit geology

The Golden Triangle region is located in the southwestern part of the Yangtze Craton. It encompasses the northern Nanpanjiang fold belt formed by convergent tectonics between the Indochina and the South China Blocks in the Triassic (Yin and Nie 1996). The Zhesang Carlin-type gold deposit occurs in the Funing County of Yunnan Province. This deposit contains a proven gold reserve of ~20 t at an average grade of 4 g t^{-1} Au. It is a representative Carlin-type gold deposit in the region (Fig. 1). Regionally, the folded strata are composed of Devonian–Permian limestones, sandstones and mudstones, and minor Triassic clastic sedimentary rocks (Fig. 2). Rare Permian mafic sills and dykes with zircon U-Pb ages of ~260 Ma related to the Emeishan mantle plume are also present in this region (Zhou et al. 2006). The gold mineralization occurs in the northeast-trending fault zones within the Permian calcareous clastic sedimentary rocks of the Wujiaping Formation or in the contacts between the Permian mafic sills/dykes and the Triassic clastic sedimentary rocks of

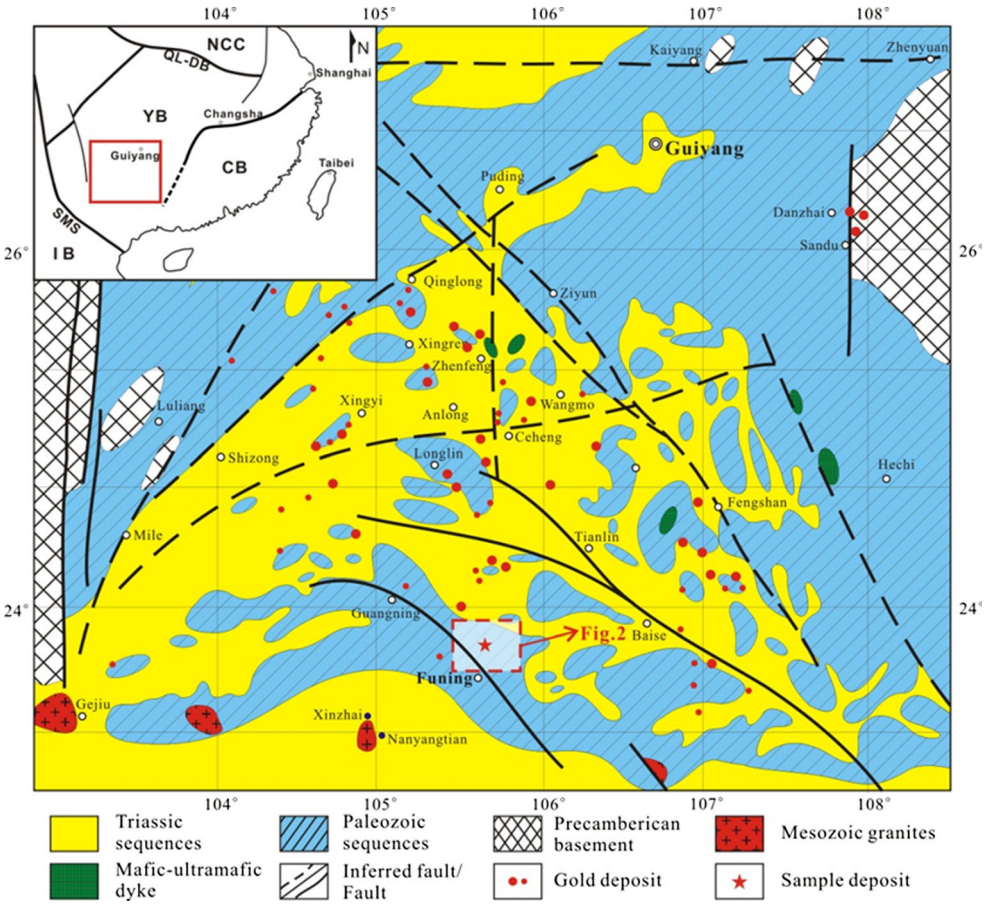

Fig. 1 Distribution of the Carlin-type gold deposits in the Golden Triangle region in SW China (modified from Hu and Zhou 2012). *NCC* North China Craton, *QL-DB* Qingling-Dabie orogenic belt, *YC* Yangtze Craton, *CB* Cathaysian Block, *SMS* Songma Suture, *IB* Indochina Block

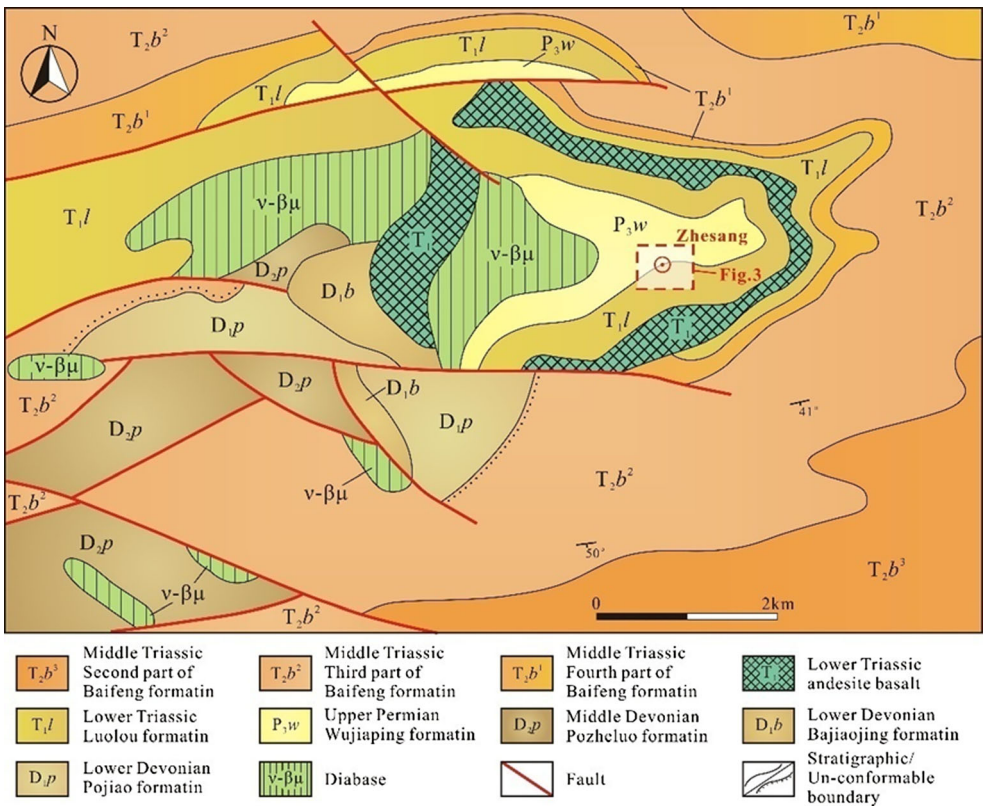

Fig. 2 Regional geological map of the Zhesang gold deposit (modified from Dai et al. 2014)

the Luolou Formation. The deposit consists of eight ore bodies. Two of them, III and VIII, occur in the contacts (Fig. 3).

Hydrothermal alteration associated with gold mineralization in the deposit includes silicification, carbonatization, sericitization, and sulfidation. The sulfide assemblages are predominately composed of arsenian pyrite and arsenopyrite that host invisible gold. The gangue minerals include quartz, calcite, and dolomite. The occurrences of gold and style of alteration are very similar to other Carlin-type gold deposits in the region (Hu et al. 2002; Su et al. 2008, 2012). Based on fluid inclusion data, the formed T-P conditions of the Zhesang Carlin-type gold deposit were estimated to be between ~100 and 250°C, and between 11 and 59 bars that correspond to the lithological depths between 200 and 2200 m (Dai et al. 2014). Based on detailed studies of fluid inclusions, however, Dong et al. (2016) suggested that the highest metallogenic temperature for the Carlin-type gold deposit hosted in contact between mafic and sedimentary rocks was higher than 300°C.

Rutile crystals are present in the altered, mineralized mafic igneous rocks within orebody III. They are the integral components of the Au-bearing arsenopyrite and pyrite assemblages. The rutile grains are yellow-brown and up to 1500 μm in length. Most of them have lengths around 500 μm (Fig. 4). The associated arsenopyrite and pyrite contain Au between 210 and 840 ppm (Table 1). The Zr contents of the hydrothermal rutile crystals, determined by in situ LA-ICP-MS method, are from 11 to 20 ppm (Table 2), which are one order of magnitude lower than the concentrations of Zr in igneous rutile crystals in the fresh mafic dykes in the region (278 to 5820 ppm). Using the Zr-in-rutile thermometer of Zack et al. (2004a), the crystallization temperatures of the hydrothermal rutile crystals in the orebody III of the Zhesang Carlin-type gold deposit were estimated to be between 290 and 375°C. In contrast, the crystallization temperatures of the igneous rutile crystals in the fresh mafic dykes were estimated to be between 730 and 1230°C.

Sampling and analytical methods

Rutile crystals were identified in the polished thin sections of a mineralized mafic dyke sample (ZSH-07) from the orebody III of the Zhesang Carlin-type gold deposit. The rutile grains then were separated from the whole rock using heavy liquids and magnetic separation, and hand-picking under a microscope. The selected grains were mounted in epoxy resin disks together with the DXK rutile standard ($^{206}Pb/^{238}U$ age = 1782.6 ± 2.8 Ma, Li et al. 2013) and an in-house rutile mega-crystal standard (JDX; $^{206}Pb/^{238}U$ age = 518 ± 4 Ma; Li et al. 2013), and then polished, cleaned, and gold-coated for in situ chemical and isotopic measurements.

Major and trace element compositions and back-scattered electron images of rutile, pyrite, and arsenopyrite were

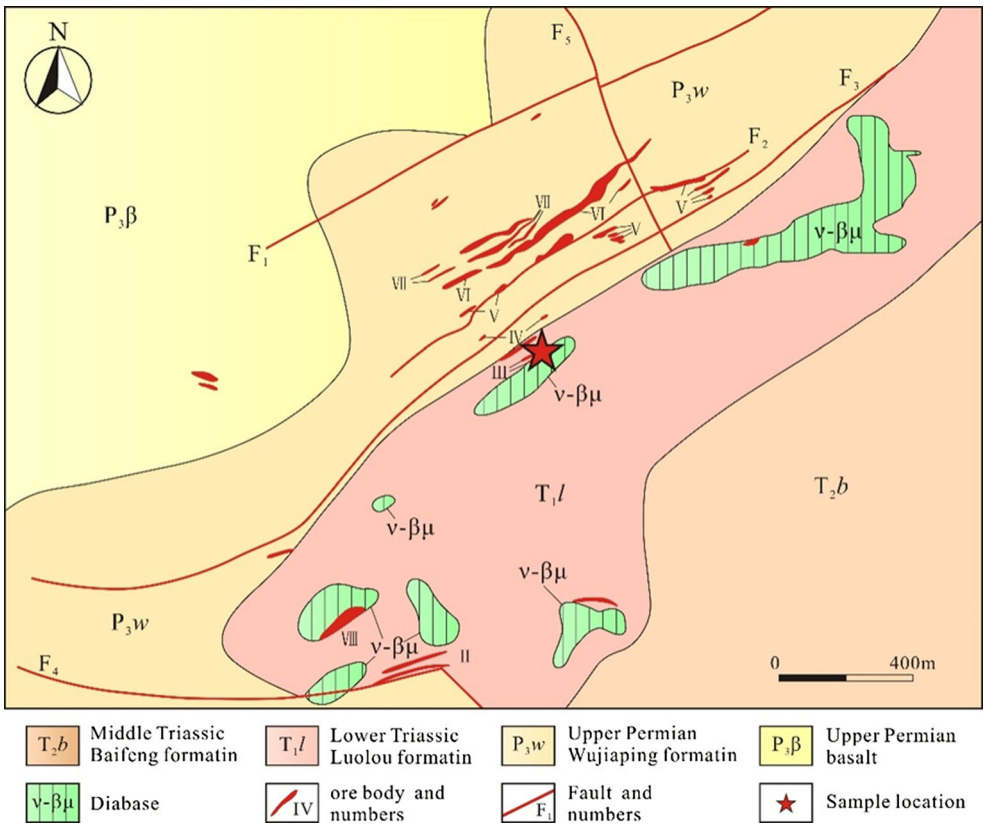

Fig. 3 Geological map of the Zhesang gold deposit (modified from Dai et al. 2014)

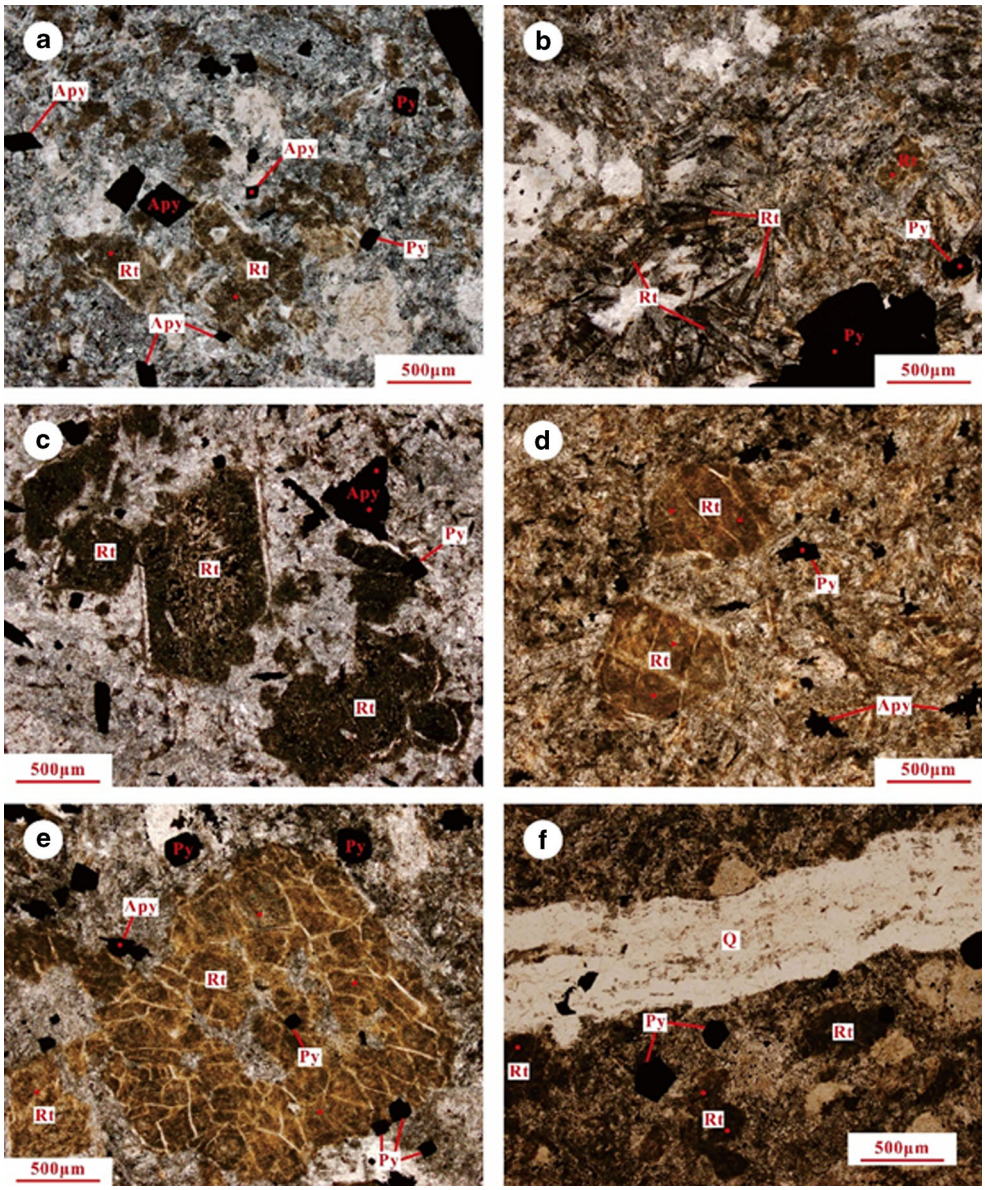

Fig. 4 Photomicrographs of rutile in the hydrothermally altered mafic dyke of the Zhesang gold deposit. **a**–**f** Rutile intergrowth with gold-bearing sulfide assemblages and **e** gold-bearing pyrite in rutile crystal. *Apy* arsenopyrite, *Py* pyite, *Rt* rutile, *Q* quartz. *Red point* stands for the location of EMPA analysis

Table 1 Compositions of pyite and arsenopyrite from the Zhesang gold deposit (wt%)

No.	Mineral	As	Ag	Co	Ni	Au	S	Fe	Cu	Total
1	Apy	40.15	0.01	0.01	0.01	0.04	22.63	34.16	0.02	97.03
2	Apy	41.57	0	0.01	0.03	0.08	21.95	34.10	0.01	97.85
3	Apy	42.33	0	0	0.01	0.03	22.35	34.19	0.03	98.96
4	Apy	39.66	0	0.01	0.01	0.03	23.75	34.43	0	97.92
5	Apy	43.55	0	0.01	0	0.03	21.46	33.55	0	98.62
6	Apy	40.06	0	0	0	0.03	23.33	34.39	0.01	97.84
7	Apy	41.31	0.02	0	0	0.05	22.33	34.36	0.01	98.18
8	Apy	42.65	0	0.08	0.44	0.08	20.99	33.39	0	97.76
9	Py	5.77	0.06	0.12	0.01	0.03	47.26	44.25	0.02	97.51
10	Py	5.05	0	0.03	0.06	0.07	47.31	45.40	0.05	97.97
11	Py	3.17	0	0.01	0.01	0.02	49.02	45.91	0.01	98.14

Table 2 Compositions of rutile from the Zhesang gold deposit (wt%, Zr in ppm)

No.	WO_3	SrO	TiO_2	PbO	UO_2	V_2O_3	Cr_2O_3	FeO	Zr	Total
1	0.36	0.04	97.61	0.02	0.01	1.74	0.05	0.21	nd	100.05
2	4.67		91.90			1.74	0.12	0.70	13.1	99.13
3	1.16		94.51	0.03		1.50	0.14	0.34	15.8	97.70
4	2.55		95.23	0.05		1.31	0.17	0.36	18.0	99.72
5	0.66		97.12		0.02	1.57	0.22	0.36	18.8	99.94
6	2.50		94.91	0.01		1.33	0.06	0.28	16.3	99.16
7	2.73		93.97			1.26	0.34	0.29	14.5	98.61
8	0.39		95.53		0.03	1.98	0.19	0.04	11.8	98.16
9	3.17		95.20	0.02		1.28	0.48	0.35	10.5	100.50
10	3.38		93.84	0.01		1.27	0.06	0.56	19.8	99.14
11	0.49	0.07	97.88	0.05		1.53	1.02	0.03	19.7	101.06
12	5.02		92.92	0.09	0.14	1.89	1.03	0.44	14.1	101.57
13	5.00		91.83			1.61	0.61	0.53	19.5	99.57
14	4.77	0.01	91.15	0.01		1.76	0.65	0.47	16.2	98.81
15	0.55		95.66		0.01	1.50	0.84	0.03	11.2	98.68
16	4.37		94.73	0.03	0.04	1.27	0.67	0.61	nd	101.73
17	0.39		98.95	0.02	0.10	1.20	0.31	0.22	18.9	101.23
18	5.62		91.26	0.02	0.02	1.32	2.22	0.17	15.2	101.65
19	4.79		93.94	0.04		1.53	0.58	0.63	11.9	101.50
20	5.02		93.13	0.05		1.55	0.92	0.58	nd	101.24
21	4.22		94.76	0.04		1.29	0.77	0.55	nd	101.62
22	0.60		96.59		0.02	1.46	0.77	0.02	nd	99.45
23	4.84		93.06			1.60	0.93	0.45	nd	100.88
24	3.12		93.47		0.02	1.42	0.82	0.26	nd	99.11
25	4.34	0.03	93.47		0.01	1.86	0.71	0.34	nd	100.755

Blank is below detection limit

nd not determined

acquired using a JOEL-8230 electron microprobe at Guilin University of Technology. Quantitative analysis was carried out using the X-ray wavelength dispersive spectrometry, whereas mineral identification was done using the energy dispersive X-ray patterns. The compositions of arsenopyrite were determined under the conditions of 25-keV accelerating voltage, 10–40-nA beam current, and 10-s counting time. Under these conditions, the detection limit for gold is estimated to be ~400 ppm. The standards used were natural marcasite for Fe and S, GaAs (Alfa, Aesar, USA) for As, cuprite for Cu, crocoite for Cr, and native gold for Au.

Raman spectroscopy was conducted on the sample at 50–1500 cm^{-1} using a confocal laser Raman instrument (Horiba JobinYvon, LabRAM HR800, England) equipped with a full-area charge-coupled device detector and an Ar laser of 514.5 nm with an incident power 50 mW. An aqueous $NaNO_3$ saturated solution was used as reference to avoid signal fluctuation during the analysis.

The measurements of U–Pb isotopes of rutile were performed using a CAMECAIMS-1280 ion microprobe in the Institute of Geology and Geophysics, Chinese Academy of Sciences in Beijing. The instrumental conditions and measurement procedures were similar to those given in Li et al. (2011). AnO_2^- primary-ion beam was accelerated at 13 kV with an intensity of ~15 nA. The aperture illumination mode (Kohler illumination) was used with a ~200-μm aperture to produce even sputtering over the entire analyzed area. The ellipsoidal spot was approximately 20 × 30 μm in size. Positive secondary ions were extracted with a 10-kV potential. A mass resolution of ~7000 was used, and the magnet was cyclically peak-stepped to capture the signals of $^{206}Pb^+$, $^{207}Pb^+$, $^{208}Pb^+$, U^+, UO^+, ThO^+, UO^{2+}, and $^{49}TiO_4{}^+$. A single ion-counting electron multiplier was used as the detection device. Each measurement comprises 10 cycles during a total analytical duration of ~15 min, including 2-min rastering prior to the actual analysis to reduce the contribution of surface contaminant Pb. Baseline was measured before each session to make sure the good analytical conditions. The normal baseline is <0.01 cps on the EM, which is negligible for all the signals. DXK rutile was used as the standard to calibrate the Pb/U

fractionation, and JDX rutile as an unknown to monitor the whole analytical procedure. The uncertainty of Pb/U ratio for single spot is a combination of the standard deviation of calibration curve from the DXK standards and the internal precision. The uncertainty of Pb/Pb ratio is from the internal precision. The U–Pb isotopic ages were calculated using the decay constants recommended by Sterger and Jäger (1977) and the Isoplot/Ex software (Ludwig 2003). The reported results have 95% confidence in accuracy.

Results

Rutile texture and composition

Laser micro-Raman spectroscopy was used to identify the mineral polymorphs of TiO_2 minerals. A compilation of Raman spectrum for standard TiO_2 minerals (brookite, anatase, and rutile; Meinhold 2010) is shown in Fig. 6. Rutile is characterized by the peaks at wavenumbers 143, 247, 447, and 612 cm^{-1}, anatase by the peaks at wavenumbers 144, 197, 400, 516, and 640 cm^{-1}, and brookite by the peaks at wavenumbers 153, 247, 322, and 636 cm^{-1} (Porto et al. 1967; Meinhold 2010). The spectrum shows that the TiO_2 mineral from the Zhesang Carlin-type gold deposit (ZSH-7-1) is most similar to rutile (Fig. 5).

Table 2 shows the chemical compositions of the selected rutile crystals from the Zhesang Carlin-type gold deposit, determined by EPMA (Zr by LA-ICP-MS). The rutile crystals studied contain 91.15 to 97.61 wt% TiO_2, with minor WO_3, Cr_2O_3, Nb_2O_5, V_2O_3, and FeO. The abundance of WO_3 ranges from 0.36 to 5.62 wt%, with a mean value of 2.95 wt%. The abundance of V_2O_3 varies from 1.21 to 1.98 wt%, with a mean value of 1.5 wt%. The abundance of Cr_2O_3 is from 0.05 to 2.22 wt%, with a mean value of 1.10 wt%. The abundance of Zr is from 10.5 to 19.8 ppm, with a mean value of 16.4 ppm.

SIMS U-Pb data for rutile

A total of twenty-seven measurements were conducted on the selected rutile crystals from the Zhesang Carlin-type gold deposit. The U–Pb data for the selected rutile grains are listed in Table 3 and illustrated in Fig. 6. The measured U contents range from 4 to 27 ppm, mostly close to 10 ppm (Table 3). The proportions of common lead are high, with f_{206} values varying between 65 and 89%. On the Tera–Wasserburg plot constructed with the total Pb composition and total Pb/U ratio, linear regression of the data points (MSWD = 0.95) gives a lower intercept age of 213.6 ± 5.4 Ma (2σ) and the upper intercept of $^{207}Pb/^{206}Pb$ = 0.86 ± 0.06 for the common Pb (Fig. 6).

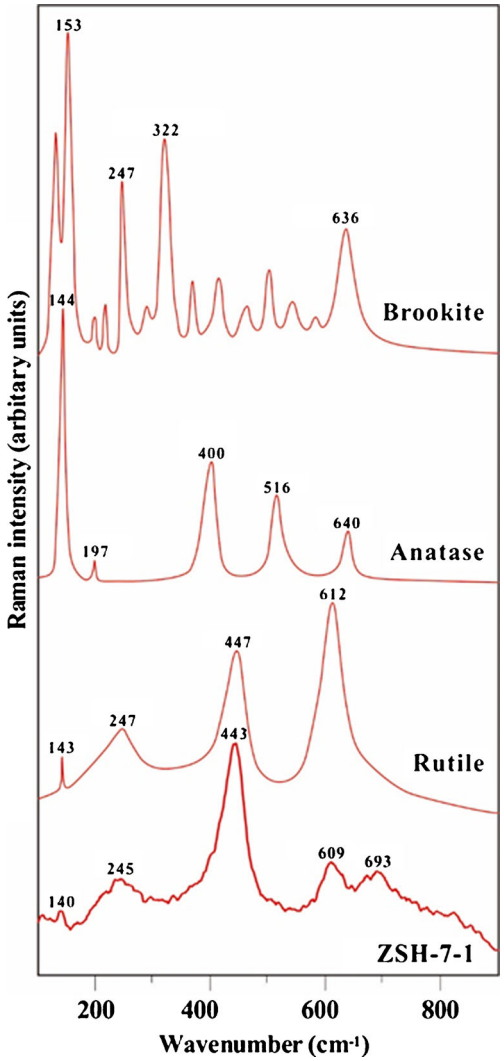

Fig. 5 Comparison of Raman spectra between the standard TiO_2 minerals (brookite, anatase, and rutile; Meinhold 2010) and ZSH-7-1 from the Zhesang gold deposit

Discussion

Precipitation of rutile during gold mineralization

There are several possible and common substitutions for titanium in rutile, such as Al, V, Cr, Fe, Zr, Nb, Sn, Sb, Hf, Ta, W, and U (Bromiley and Hilairet 2005; Carruzzo et al. 2006). These elements may be used to trace the source for rutile (Rudnick et al. 2000; Zack et al. 2002; Zack et al. 2004a, b; Clark and Williams-Jones 2004; Scott 2005; Scott and Radford 2007). The high-field strength elements such as Nb and Ta may be used to identify an igneous protolith formed by subduction-related magmatism (Rudnick et al. 2000). The Cr and Nb abundances in rutile can also be used to identify source lithologies, such as metapelitic versus metamafic rocks (Zack et al. 2002, 2004b). Rutile from hydrothermal metallic ore deposits is commonly characterized by high abundances

Table 3 Rutile U–Pb data analyzed by Cameca IMS-1280 ion microprobe (U and Th in ppm)

Sample/spot	U	Th/U	$^{238}U/^{206}Pb$	±σ%	$^{207}Pb/^{206}Pb$	±σ%	$T_{207/206}$ Age (Ma)	±σ	f_{206}
Sample ZSH-07									
ZSH -07@100	9	26.1	7.563	5.0	0.6449	1.5	222.6	27.3	0.75
ZSH -07@105	25	24.9	6.391	6.7	0.6752	1.2	226.3	33.6	0.78
ZSH -07@107	4	23.7	8.155	5.9	0.6069	1.8	242.7	26.5	0.70
ZSH -07@110	6	25.9	7.986	4.6	0.6499	1.7	206.0	26.3	0.75
ZSH -07@112	15	26.6	5.787	3.6	0.6929	1.5	225.9	36.3	0.80
ZSH -07@114	21	25.0	7.611	3.6	0.6335	1.6	232.8	26.1	0.73
ZSH -07@116	7	23.9	3.301	3.0	0.7771	1.0	196.8	67.8	0.90
ZSH -07@120	9	23.1	9.414	4.2	0.5999	2.1	216.3	22.0	0.69
ZSH -07@123	9	17.7	9.755	3.6	0.6169	1.1	195.3	19.3	0.71
ZSH -07@17	6	22.0	7.256	4.5	0.6644	2.0	211.1	30.2	0.77
ZSH -07@18	4	23.3	11.632	3.7	0.5593	1.9	202.6	16.6	0.65
ZSH -07@34	7	22.9	7.830	6.1	0.6255	1.7	234.2	27.8	0.72
ZSH -07@4	12	19.6	10.332	4.8	0.5805	2.3	211.9	20.8	0.67
ZSH -07@40	7	16.3	7.114	6.1	0.6915	1.9	185.8	32.5	0.80
ZSH -07@44	11	21.7	8.429	3.7	0.6306	1.2	213.1	22.8	0.73
ZSH -07@46	5	18.9	7.781	3.3	0.6398	2.3	221.5	27.9	0.74
ZSH -07@51	6	25.3	7.427	5.6	0.6396	1.6	232.1	28.8	0.74
ZSH -07@53	5	31.4	6.725	4.1	0.6795	1.3	210.2	30.5	0.79
ZSH -07@56	5	22.0	9.849	3.3	0.5989	2.0	207.6	20.1	0.69
ZSH -07@58	8	20.8	7.638	6.8	0.6426	1.6	222.8	29.0	0.74
ZSH -07@62	6	14.4	3.309	3.6	0.7626	1.3	230.3	68.3	0.88
ZSH -07@75	19	23.9	4.450	3.8	0.7525	0.8	189.4	48.2	0.87
ZSH -07@76	11	24.9	6.695	4.3	0.6727	1.5	219.0	31.1	0.78
ZSH -07@78	7	25.2	8.804	4.8	0.6338	1.7	201.3	23.7	0.74
ZSH -07@96	10	24.3	8.859	6.2	0.6187	1.4	213.3	24.1	0.72
ZSH -07@98	8	20.3	6.738	6.1	0.6580	1.5	234.5	32.1	0.76
ZSH -07@99	9	23.4	8.311	4.7	0.6379	2.0	209.3	25.9	0.74

of W, V, Sr, Cu, Sn, and Sb, which can be used to distinguish hydrothermal rutile crystals from those in igneous and metamorphic rocks (Clark and Williams-Jones 2004; Scott 2005, Scott and Radford 2007).

The rutile crystals in the Zhesang Carlin-type gold deposit are enriched in W (WO_3, 0.36–5.62 wt%) and V (V_2O_3, 1.20–1.98 wt%) (Table 2). High W concentrations in the rutile crystals might indicate the involvement of hydrothermal fluids during rutile precipitation (Clark and Williams-Jones 2004). High V in rutile is a good indicator of hydrothermal origin (Scott 2005). The observed high concentrations of W and V indicate that the rutile crystals from the Zhesang Carlin-type gold deposit are of hydrothermal origin. This is also supported by their low Zr concentrations and low estimated crystallization temperatures between 290 and 375°C as described above.

Clark and Williams-Jones (2004) summarized the Ti, Fe, Cr, V, and W contents of rutile from various metamorphosed hydrothermal gold deposits, from which the hydrothermal

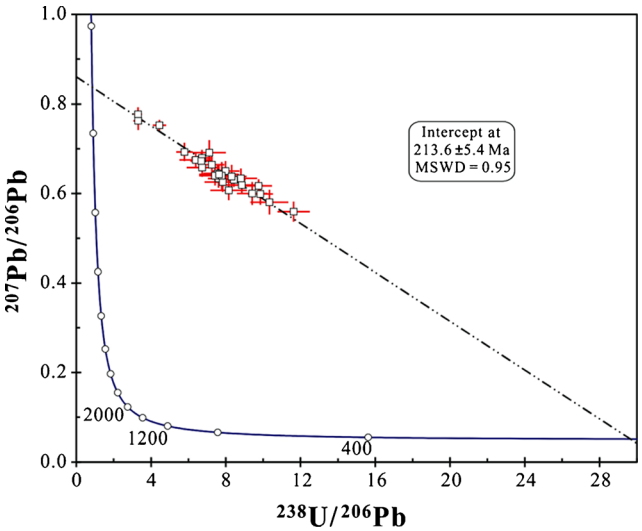

Fig. 6 Tera-Wasserburg plot for U–Pb data of rutile crystals from the Zhesang gold deposit

rutile in ores and altered rocks could be clearly distinguished from those in unaltered fresh wallrocks (Fig. 7). The observed concentrations of these elements in rutile from the Zhesang Carlin-type gold deposit are consistent with the interpretation of a hydrothermal origin for the rutile (Fig. 7). Other evidence for a hydrothermal origin of the selected rutile crystals from the Zhesang Carlin-type gold deposit includes their occurrences as intergrowths with the gold-bearing sulfides (Fig. 4) and the presence of gold-bearing pyrite in some of the selected rutile crystals (Fig. 4e), further indicating that the rutile precipitated together with gold mineralization. Therefore, the 213.6 ± 5.4 Ma U-Pb isotope age of the selected rutile crystals can be regarded as the crystallization age of rutile from the gold-bearing hydrothermal fluid or the recrystallization age of rutile during the interaction between the gold-bearing hydrothermal fluids and the mafic dyke. Either way, the rutile U-Pb age of 213.6 ± 5.4 Ma can be used to represent the formation age of the deposit.

Comparison of different dating methods for Carlin-type gold deposits

A number of isotopic dating methods, mainly including pyrite Rb-Sr and Re-Os, sericite ^{40}Ar–^{39}Ar, and inclusion-fluid Rb-Sr, have been applied to the Carlin-type gold deposits in the Golden Triangle, SW China. The results from the various types of methods do not agree with each other very well and have hampered our understanding of ore genesis for this type of deposits (Hu et al. 1995, 2002; Su et al. 1998, 2009a; Zhang and Yang 1992; Chen et al. 2009, 2015). As pointed out briefly above, the Rb-Sr isochron methods of pyrite and fluid inclusions are not reliable and should all be abandoned.

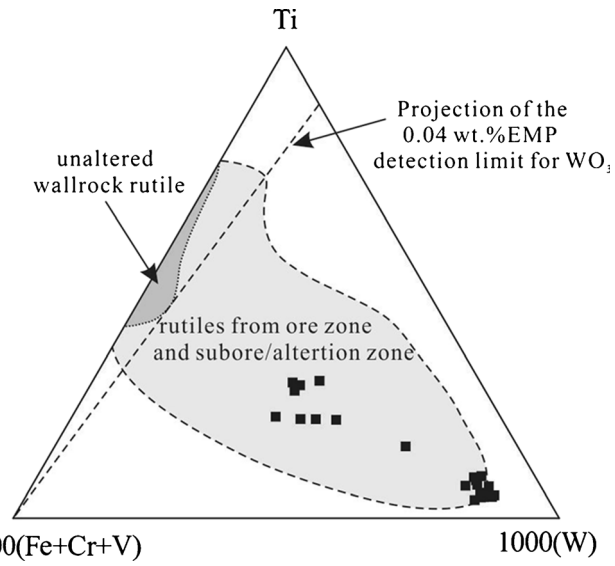

Fig. 7 Summary of Ti, Fe, Cr, V, and W contents of rutile from hydrothermal gold deposits. The *black solid squares* were the plots of rutile from orebody III of the Zhesang gold deposit. The two shadow fields are from Clark and Williams-Jones (2004)

Au-bearing pyrite in the Carlin-type gold deposits is commonly zoned, with a core formed in the diagenetic stage of sedimentary rocks and an Au-bearing arsenian pyrite ring formed in the Au precipitation stage from hydrothermal fluids (Hofstra and Cline 2000; Hu et al. 2002; Cline et al. 2005; Su et al. 2008). As a result, pyrite Re–Os and Rb-Sr isotopic dating commonly yield a mixing age, not the true age for the crystallization of the rim that formed during gold mineralization. The large errors of the pyrite Re-Os and Rb-Sr isotope ages for the Carlin-type gold deposits in the Golden Triangle region in SW China underscore this problem.

^{40}Ar–^{39}Ar dating of sericite is widely used for the study of Carlin-type gold deposits. In Nevada, this method has produced a large number of different ages that are difficult to interpret (Arehart et al. 2003). The reason is probably due to the fact that sericite alteration can be primary (Au mineralization) as well as secondary (hydrothermal overprinting or post-ore thermal perturbation). As a result, the ^{40}Ar–^{39}Ar ages of sericite crystals must be interpreted with extreme caution (Arehart et al. 2003).

In situ U-Pb dating of hydrothermal rutile is clearly a promising new method for any type of hydrothermal deposits including Carlin-type gold deposits as long as this phase is present in the mineralization assemblages. As described above, our new rutile U-Pb age of 213.6 ± 4.6 Ma for the Zhesang Carlin-type gold deposit is within the range of the previously reported Re–Os isochron ages of arsenopyite crystals from three other Carlin-type gold deposits in the region (204 ± 19 to 235 ± 33 Ma; Chen et al. 2015). However, the error for the rutile U-Pb age is significantly lower.

Geodynamic setting of gold mineralization

It is very interesting that the ages of the Carlin-type gold deposits in the Golden Triangle region are similar to those of W–Sn deposits and the associated S-type granitoids in the surrounding region. The molybdenite Re–Os isotope ages for the W–Sn deposits and the zircon U-Pb isotope ages for host granite plutons vary similarly between 205 and 230 Ma (Cai et al. 2006; Ding et al. 2005; Wang et al. 2005, 2007; Wei et al. 2007; Feng et al. 2011; Hu and Zhou 2012; Mao et al. 2013).

Previously, the Carlin-type gold deposits in the Golden Triangle region were thought to be temporally related to the Yanshanian Orogeny (Hu et al. 2007; Mao et al. 2013, and references therein), which resulted from the westward subduction of the Paleo-Pacific plate (Mao et al. 2013; Su et al. 2009a, b). Our new rutile U-Pb isotopic age for the Zhesang gold deposit and the recently reported arsenopyite Re-Os isochron ages for the Shuiyindong, Jinya, and Lannigou Carlin-type gold deposits (Chen et al. 2015) in the Golden Triangle are inconsistent with such interpretation.

Instead, a genetic link to the Indosinian (Triassic) Orogeny is inferred.

The Indosinian Orogeny in South China occurred approximately at 254–242 Ma (Carter et al. 2001; Cai et al. 2006). The E–W-trending folds in the Golden Triangle region are the result of N-S compression tectonics during the Indosinian Orogeny (Xu et al. 1992; Zhang and Jiang 1994). The southwest margin of the South China Block experienced substantial horizontal shortening during the continental collision between the Indochina and the South China Blocks (Wang et al. 2005, 2007). The collision occurred between 258 ± 6 and 243 ± 5 Ma, resulting in significant crustal thickening and the closure of the Paleotethys Ocean at ~245 Ma (Carter et al. 2001; Lepvrier et al. 2004). The Indosinian Orogeny also produced abundant granitoids in the southeastern parts of the South China Block (Wang et al. 2005; Zhou et al. 2006).

Triassic peraluminous granitoids with ages ranging from 205 to 252 Ma are widespread in the Cathaysian Block, forming a prominent E-W-trending granite belt (Zhou et al. 2006). Zhou et al. (2006) proposed that the Early-Middle Triassic granite plutons in this belt are syn-collisional, whereas the Middle-Late Triassic granite plutons are post-collisional. The post-collisional peraluminous granite plutons (~230–205 Ma) are significantly younger than the Indosinian Orogeny and the associated regional metamorphism (~254–242 Ma), consistent with an extensional tectonic setting after collision.

Two granite-related W-Sn deposits (the Xinzai Sn deposit and the Nanyangtian W deposit; Fig. 1) with a similar age of ~210 Ma occur ~100 km west of the Zhesang Carlin-type gold deposit (Feng et al. 2011). It is possible that the Middle-Late Triassic granite plutons that formed in a post-collisional extensional tectonic setting are also present in the Golden Triangle region at depth but have not been exposed on the surface. We further postulate that the formation of the Carlin-type gold deposits in the Golden Triangle region is linked to such tectonic-magmatic event, similar to the model that was proposed for the Carlin-type gold deposits in Nevada (Cline et al. 2005; Muntean et al. 2011).

Conclusions

Hydrothermal rutile intergrown with gold-bearing sulfides is present in the Zhesang Carlin-type gold deposit in the Golden Triangle region in SW China. The rutile crystals yielded a U-Pb age of 213.6 ± 5.4 Ma, which is interpreted to represent the timing of gold precipitation from the Zhesang hydrothermal system. This age is within the range of hydrothermal W-Sn deposits and the associated S-type granitoids in the surrounding regions.

Our new age data show that the Indosinian (Triassic) gold mineralization in the Golden Triangle region in SW China was not related to the westward subduction of the Paleo-Pacific plate. Instead, it might be linked to the emplacement of coeval, widespread granite plutons in an extensional tectonic setting after the collision between the Indochina and the South China Blocks.

The results from this study indicate that U–Pb dating of hydrothermal rutile is a promising tool to determine the ages of a variety of hydrothermal deposit including Carlin-type gold deposits so long as it is present in the deposits.

Acknowledgements Many thanks go to Dr. Xianhua Li of the Institute of Geology and Geophysics, Chinese Academy of Sciences, for his assistance in rutile isotope measurements. We are grateful to Dr. Chusi Li of Indiana University for revising the manuscript, and to two anonymous reviewers for their thoughtful reviews. This research was supported jointly by the key project of the National Natural Science Foundation of China (41230316), the National "973" Program of China (2014CB440906), and the National Science Foundation of China (41563004, 41172089).

References

Arehart GB, Chakurian AM, Tertbar DR (2003) Evaluation of radioisotope dating of Carlin-type deposits in the Great Basin, Western North America, and implications for deposit genesis. Econ Geol 98:235–248

Bibikova E, Skiold T, Bogdanova S, Gorbatschev R, Slabuno A (2001) Titanite–rutile thermochronometry across the boundary between the Archaean craton in Karelia and the Belomorian Mobile Belt, eastern Baltic shield. Precambrian Res 1053:15–33

Bromiley GD, Hilairet N (2005) Hydrogen and minor element incorporation in synthetic rutile. Miner Mag 69:345–358

Cai MH, Chen KX, Qu WJ, Liu GQ, Fu JM, Yin JP (2006) Geological characteristics and Re–Os dating of molybdenites in Hehuaping tin–polymetallic deposit, southern Hunan province. Miner Deposits 25: 263–268 (in Chinese with English abstract)

Carruzzo S, Clarke DB, Pelrine KM, MacDonald MA (2006) Texture, composition, and origin of rutile in South Mountain batholith, Nova Scotia. Can Mineral 44:715–729

Carter A, Roques D, Bristow C, Kinny P (2001) Understanding Mesozoic accretion in Southeast Asia: significance of Triassic thermotectonism (Indosinian orogeny) in Vietnam. Geology 29: 211–214

Chakurian AM, Arehart GB, Donelick RA (2003) Timing constraints of gold mineralization along the Carlin trend utilizing apatite fission-track, $^{40}Ar/^{39}Ar$, and apatite (U-Th)/He methods. Econ Geo l98: 1159–1171

Chen MH, Huang QW, Hu Y, Chen ZY, Zhang W (2009) Genetic types of phyllosilicate (micas) and its $^{39}Ar–^{40}Ar$ dating in Lannigou gold deposit, Guizhou Province, China. Acta Mineral Sin 29:353–362 (in Chinese with English abstract)

Chen MH, Mao JW, Li C, Zhang ZQ, Dang Y (2015) Re–Os isochron ages for arsenopyrite from Carlin-like gold deposits in theYunnan–Guizhou–Guangxi "golden triangle", southwestern China. Ore Geol Rev 64:316–327

Clark JR, Williams-Jones AE (2004) Rutile as a potential indicator mineral for metamorphosed metallic ore deposits. Rapport Final de DIVEX, Sous-projet SC2, Montréal, Canada. 17

Cline JS, Hofstra AH, Muntean JL(2005) Carlin-type gold deposit in Nevada: critical geological characteristics and viable model. Econ Geol 100th Anniversary Volume: 451–484

Dai HZ, Chen CH, Gu XX, Li BH, Dong SY, Cheng WB (2014) Characteristics of ore-forming fluids from Zhesang gold deposit in Funing County, Yunnan Province. Geoscience 28(5):893–904 (in Chinese with English abstract)

Ding X, Chen PR, Chen WF, Huang HY, Zhou XM (2005) LA-ICPMS zircon dating of Weishangranitic plutons in HunanProvince: petrogenesis and tectonic implications. Sci Chin Ser D Earth Sci 35(7): 606–616

Dong WD,Su WC, Sheng NP, Cai JL (2016) Study on the ore-forming fluid geochemistry of the Anna gold deposit in southeastern Yunnan province, China. Acta Petrol Sin (in press, in Chinese with English abstrct)

Doyle MG, Fletcher IR, Foster J, Large RR (2015) Geochronological constraints on the Tropicana gold deposit and Albany-Fraser orogen, Western Australia. Econ Geol 110:355–386

Feng JR, Mao JW, Pei RF, Li C (2011) A tentative discussion on Indosinian ore-forming events in Laojunshan area of southeasternYunnan: a case study of Xinzhai tin deposit and Nanyangtian tungsten deposit. Mineral Deposits 30:57–73 (in Chinese with English abstract)

Hall CM, Kesler SE, Simon G (2000) Overlaping cretaceous and Eocene alteration, twin Greeks Carlin-type deposits, Nevada. Econ Geol 95: 1739–1752

Hirdes W, Davis DW (2002) U–Pb zircon and rutile metamorphic ages of Dahomeyan garnet-hornblende gneiss in southeastern Ghana, West Africa. J Afr Earth Sci 35:445–449

Hofstra AH, Cline JS (2000) Characteristics and models for Carlin type gold deposits. Rev Econ Geol 13:163–220

Hu RZ, Zhou MF (2012) Multiple Mesozoic mineralization events in South China-an introduction to the thematic issue. Mineral Deposita 47(6):579–588

Hu RZ, Su WC, Bi XW, Li ZQ (1995) A possible evolution way of ore-forming hydrothermal fluid for the Carlin-type gold deposits in the Yunnan-Guizhou-Guangxi triangle area. Acta Miner Sin 15:144–149 (in Chinese withEnglish abstract)

Hu RZ, Su WC, Bi XW, Tu GZ, Hofstra AH (2002) Geology and geochemistry of Carlin-type gold deposits in China. Mineral Deposita 37:378–392

Hu RZ, Peng JT, Ma DS, Su WC, Shi CH, Bi XW, Tu GZ (2007) Epoch of large-scale low-temperature mineralizations in southwestern Yangtze massif. Miner Deposits 26(6):583–596 (in Chinese with English abstract)

Hu RZ, Bi XW, Jiang GH, Chen HW, Peng JT, Qi YQ, Wu LY, Wei WF (2012a) Mantle-derived noble gases in ore-forming fluids of the granite-related Yaogangxian tungsten deposit, southeastern China. Mineral Deposita 47(6):623–632

Hu RZ, Wei WF, Bi XW, Peng JT, Qi YQ, Wu LY, Chen YW (2012b) Molybdenite Re-Os and muscovite $^{40}Ar/^{39}Ar$ dating of the Xihuashan tungsten deposit, central Nanling district, South China. Lithos 150:111–118

Kesler SE, Riciputi LC, Ye ZJ (2005) Evidence for a magmatic origin for Carlin-type gold deposits:isotopic composition of sulfur in the Betze-post-screamer deposit, Nevada, USA. Mineral Deposita 40: 127–136

Kooijman E, Mezger K, Berndt J (2010) Constraints on the U-Pb systematics of metamorphic rutile from in situ LA-ICP-MS analysis. Earth Planet Sci Lett 293:321–330

Lepvrier C, Maluski H, Vu VT, Leyreloup A, Phan TT, Nguyen VV (2004) TheEarly Triassic Indosinian orogeny in Vietnam (Truong Son Belt and Kontum massif): implications for the geodynamic evolution of Indochina. Tectonophysics 393:87–118

Li QL, Li S, Zheng YF, Li H, Massonne HJ, Wang Q (2003) A high precision U–Pb age of metamorphic rutile in coesite-bearing eclogite from the Dabie Mountains in centralChina: a new constraint on the cooling history. Chem Geol 200:255–265

Li QL, Lin W, Su W, Li XH, Shi YH, Liu Y, Tang GQ (2011) SIMS U-Pb rutile age of low-temperature eclogites from southwestern Chinese Tianshan. NW China Lithos 122:76–86

Li QL, Yang YN, Shi YH, Lin W (2013) Eclogite rutile U-Pb dating: constrant for formation and evolution of continental collisional orogen. Chin Sci Bull 58:2279–2284

Ludwig KR (2003) User's Manual for Isoplot/Ex, Version 3.00, A Geochronological Toolkit for Microsoft Excel. Berkeley Geochronology Center Special Publication, Berkeley

Mao JW, Cheng YB, Chen MH, Pirajno F (2013) Major types and time-space distribution of Mesozoic ore deposits in South China and their geodynamic settings. Mineral Deposita 48:267–294

Meinhold G (2010) Rutile and its applications in earth sciences. Earth-Sci Rev. doi:10.1016/j.earscirev.2010.06.001

Muntean JL, Cline JS, Simon AC (2011) magmatic-hydrothermal origin of Nevada's Carlin-type gold deposits, Nature Geoscience, DOI: 10.1038/NGEO1064

Porto SPS, Fleury PA, Damen TC (1967) Raman spectra of TiO_2, MgF_2, ZnF_2, FeF_2, and MnF_2. Phys Rev 154:522–526

Rudnick RL, Barth M, Horn I, McDonough WF (2000) Rutile-bearing refractory eclogites: missing link between continents and depleted mantle. Science 287:278–281

Scott KM (2005) Rutile geochemistry as a guide to porphyry Cu–Au mineralization, Northparkes, new South Wales, Australia. Geochem Explor Environ Anal 5:247–253

Scott KM, Radford NW (2007) Rutile compositions at the big bell Au deposit as a guide for exploration. Geochem Explor Environ Anal 7: 353–361

Sterger RH, Jäger E (1977) Subcommission on geochronology; convention of the use of decay constants in geochronology and cosmochronology. Earth Planet Sci Lett 36:359–362

Su WC, Yang KY, Hu RZ, Chen F (1998) Fluid inclusion chronological study of the Carlin-type gold deposits in southwestern China: as exemplified by the Lannigou gold deposit, Guizhou province. Acta Miner Sin 18(3):359–362 (in Chinese withEnglish abstract)

Su WC, Xia B, Zhang HT, Zhang XC, Hu RZ (2008) Visible gold in arsenian pyrite at the Shuiyindong Carlin-type gold deposit, Guizhou, China: implications for the environment and processes of ore formation. Ore Geol Rev 33(3–4):667–679

Su WC, Hu RZ, Xia B, Xia Y, Liu YP (2009a) Calcite Sm-Nd isochron age of the Shuiyindong Carlin-type gold deposit, Guizhou, China. Chem Geol 258(3–4):269–274

Su WC, Heinrich CA, Pettke T, Zhang XC, Hu RZ, Xia B (2009b) Sediment-hosted gold deposits in Guizhou, China: products of wall-rock sulfidation by deep crustal fluids. Econ Geol 104(1):73–93

Su WC, Zhang HT, Hu RZ, Ge X, Xia B, Chen YY, Zhu C (2012) Mineralogy and geochemistry of gold-bearing arsenian pyrite from the Shuiyindong Carlin-type gold deposit, Guizhou, China: implications for gold depositional processes. Mineral Deposita 47(6): 653–662

Tretbar DR, Arehart GB, Christen JN (2000) Dating gold deposition in a Carlin-type gold deposit using Rb/Sr methods on the mineral galkhaite. Geology 28:947–950

Tu GC (1992) Some problems on prospecting of super large gold deposits. Acta Geol Sichuan 12:1–9 (in Chinese)

Vry JK, Baker JA (2006) LA-MC-ICPMS Pb–Pb dating of rutile from slowly cooled granulites: confirmation of the high closure temperature for Pb diffusion in rutile. Geochim Cosmochim Acta 70:1807–1820

Wang YJ, Zhang YH, Fan WM, Peng TP (2005) Structural signatures and $^{40}Ar/^{39}Ar$ geochronology of the Indosinian Xuefengshan transpressive belt, South China interior. J Struct Geol 27:985–998

Wang YJ, Fan WM, Sun M, Liang XQ, Zhang YH, Peng TP (2007) Geochronological, geochemical and geothermal constraints on

petrogenesis of the Indosinian peraluminous granites in the South China block: a case study in the Hunan Province. Lithos 96:475–502

Wei DF, Bao ZY, Fu JM, Cai MH (2007) Diagenetic and mineralization age of the Hehuaping tin–polymetallic ore field, Hunan province. Acta Geol Sin 81:244–252

Xu ZQ, Hou LW, Wang ZX (1992) The orogenic process of Songfan-Ganzi Orogenic Belt in China. Geological Publishing House, Beijing 190p (in Chinese with English abstract)

Yan DP, Zhou MF, Song HL, Wang XW, Malpas J (2003) Origin and tectonic significance of a Mesozoic multi-layer over-thrust within the Yangtze Block (South China). Tectonophysics 361:239–254

Yin A, Nie S (1996) A Phanerozoic palinspastic reconstruction of China and its neighboring regions. In: Yin A, Harrison TM (eds) The Tectonic Evolution of Asia. Cambridge University Press, Cambridge, pp 442–485

Zack T, Kronz A, Foley SF, Rivers T (2002) Trace element abundances in retiles from eclogites and associated garnet mica schists. Chem Geol 184:97–122

Zack T, Moraes R, Kronz A (2004a) Temperature dependence of Zr in rutile: empirical calibration of a rutile thermometer. Contr Miner Petrol 148:471–488

Zack T, von Eynatten H, Kronz A (2004b) Rutile geochemistry and its potential use inquantitative provenance studies. Sedi Geol 171:37–58

Zhang F, Yang KY (1992) A study on the metallogenic epoch fine disseminated gold deposit in Southwest Guizhou using the fission track. Chin Sci Bull 37:1593–1595

Zhang JQ, Jiang TC (1994) Sedimentary characteristics of Triassic back-arc basin of Youjiang and its evolution. Geol Guangxi 7:1–14 (in Chinese with English abstract)

Zhou MF, Yan DP, Kennedy AK, Li YQ, Ding J (2002) SHRIMP zircon geochronological and geochemical evidence for Neo-Proterozoic arc-related magmatism along the western margin of the Yangtze Block, South China. Earth Planet Sci Lett 196:51–67

Zhou XM, Sun T, Shen W, Shu L, Niu Y (2006) Petrogenesis of Mesozoic granitoids and volcanic rocks in South China: a response to tectonic evolution. Episodes 29:26–33